I&EC research
Industrial & Engineering Chemistry Research

pubs.acs.org/IECR

Article

Regular Solution Approach to Modeling the Supercritical Fluid Extraction of Two-Component Solutes from Ground Oilseeds

Artur A. Salamatin* and Alyona S. Khaliullina

Cite This: https://doi.org/10.1021/acs.iecr.3c01488

Read Online

ACCESS | Metrics & More | Article Recommendations

ABSTRACT: The extract obtained at supercritical fluid extraction from plant raw material is essentially multicomponent. A multicomponent mass-transfer model at the particle scale is developed to account for the non-ideality of the chemical interactions between solute components. The oil is represented by two pseudo-components, and the gradient of the chemical potential is considered the driving force for the mass transfer. The model is based on the regular solution and Gibbs energy approaches to the thermodynamic modeling of phase equilibria that take place in the raw material with a high initial oil content. The Stefan−Maxwell approach is used to balance the drag effect/chemical interactions and the driving force of diffusion in a non-equilibrium multicomponent solution. It is demonstrated that the two solute components may act as "co-solvents", thus facilitating the extraction of each other, or as "anti-solvents", thus decreasing the overall extraction rates. At least a 60% relative error in the overall flux from the particle surface is observed when the developed model is compared against a simplified approach that considers the solution as an ideal system. It is found that while the flowing fluid accumulates the extracted solute, the phase separation may take place in the pore volume of the packed bed. Possible conditions of phase separation in the pores of the packed bed are discussed.

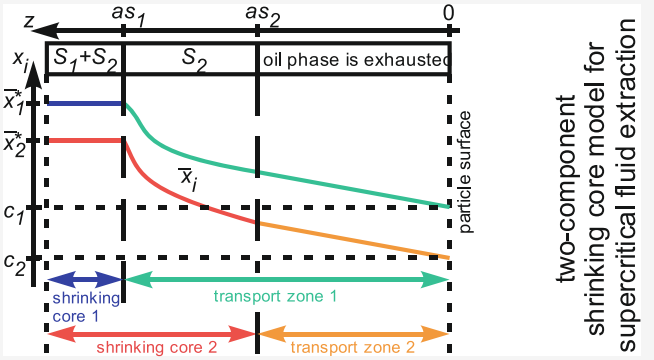

1. INTRODUCTION

The process of supercritical fluid extraction (SFE) employs fluids (solvents) at temperatures and pressures above or near the corresponding critical conditions. Carbon dioxide (CO_2) is one of the most used solvents because it is environmentally friendly and non-toxic; has a moderate critical temperature, ∼31 °C; and can be easily separated from the extract by reducing the pressure. The new technology is widely used in pharmaceutical production and in the food and biofuel industries.[1,2] The extraction of natural compounds from plant matrices (ground seeds, leaves, petals, etc.) remains one of the most common applications of the SFE process.[3−5] In particular, pumpkin,[6] rape,[7] sunflower seeds,[8,9] apricot kernels,[10] and others with a high oil content are sources of valuable natural compounds such as (un)saturated acids, e.g., triacylglycerols (TAGs), and vitamins.

Extraction under supercritical conditions takes place in a cylindrical vessel (extraction column) where particles of ground raw material are placed to form a porous packed bed. The solvent is introduced into the vessel, and the operational temperature (40−70 °C) and pressure (30−70 MPa) are set. Then, the fluid is pumped through the bed at a given flow rate under the applied pressure gradient. During the extraction process, the solvent diffuses along the internal transport channels inside the plant particles.[11−14] It penetrates into the oil-containing plant cells, dissolving the extractable oil components, which move to the surface of the ground material to be transported further by the fluid flow to the outlet cross section of the extraction column. The gradients of the chemical potentials of the non-uniformly distributed dissolved oil components inside individual particles are the driving forces of extraction.

The solute (extractable compounds) of the raw material (ground seeds) is a multicomponent mixture of organic molecules—TAGs.[15,16] Any TAG species is a set of three fatty acids esterified with a glycerol, $C_3H_5(OH)_3$. So, the species are identified by the triplet of their organic acids. The most abundant ones are palmitic (P), stearic (St), and oleic (O) acids. Consider TAGs of high-oleic sunflower oil (HOSO) and fully hydrogenated palm oil (FHPO) as typical examples. The major TAG acids of HOSO are linoleic (14−40%) and oleic (75−85%) ones followed by palmitic, stearic, and linolenic

Received: May 4, 2023
Revised: June 17, 2023
Accepted: June 22, 2023

acids and so on. The TAGs of FHPO are mainly composed of stearic (∼55%) and palmitic (∼42%) acids.

The triplets of acid molecules can esterify with glycerol in various combinations. The OOO TAG with three oleic acid molecules is the most abundant species in HOSO (∼61%). Accordingly, the TAG composition of HOSO can be viewed as a two-component mixture of OOO TAG and a pseudo-component representing all other fractions. Two major TAG components, PStSt (41.7%) and PPSt (39.3%), constitute up to ∼80% of FHPO. They are followed by StStSt (11.4%).

Mathematical models for SFE usually describe the extraction kinetics only globally, regarding the extract as a single pseudo-component. However, sophisticated SFE models are needed to better represent the multi-component nature of the solute. Such an approach was recently developed by Sovová et al.[17,18] to describe the extraction of volatile oil and cuticular waxes of *Ruta graveolens*. The authors incorporated the local equilibrium relations of Goto et al.[19] and del Valle and Urrego[20] into the thermodynamic counterpart of the model.[21] The considered type of raw material and extractable compounds are very different from the fatty oil of seeds. The volatile oil has a relatively low solute content with a larger diversity of solute molecules. The desorption processes dominate in the volatile/essential oil extraction. The model[17,18] is derived for finely ground plant material with short diffusion paths inside particles and easily accessible extract. Since some of the investigated extract components, like cuticular waxes, are found only on the particle surface,[22] the internal mass-transfer resistance has been neglected. While the assumptions are reasonable for the volatile oil extraction, they do not correspond with the seed oil extraction, where the solute is uniformly distributed within the plant material volume. So, further theoretical investigation is needed to understand and describe the fatty oil extraction processes.

In the special case of seed oil extraction, the principal mechanisms of hydrodynamic and mass-transfer phenomena in the single pseudo-component approximation are fully covered in the framework of the so-called shrinking core (SC) model.[14,23−26] The model takes into account the (1) dynamic multiphase oil distribution on the particle scale, (2) internal resistance to the solute mass transfer, and (3) high initial oil content in the raw material. According to the original, single-component SC approach, two zones exist in the particle during extraction. The outer transport zone occupies the particle volume between the particle surface and the extraction front. Here, the oil phase is exhausted, and only the solvent (or solution) phase with dissolved solute exists. The internal part of the particle volume, its core, within the extraction front contains two phases at thermodynamic equilibrium: the original single-component oil phase in plant cells and the solvent phase with the equilibrium solute content in transport channels. The two zones are separated by the sharp boundary (front) where the oil dissolution takes place. Then, the oil diffuses through the transport zone to the particle surface along the transport channels. The oil concentration decreases from the equilibrium value at the core surface to the near-zero value at the particle surface, thus maintaining the gradient of its chemical potential—the driving force of the mass transfer.

It is suggested here that multiple fronts dividing the respective cores and transport zones for individual components can be introduced to describe the multi-component extraction. Each pair of core/transport zone covers the entire particle volume. Particle parts shared among multiple cores contain a mixture of corresponding oil components. Several existing approaches[25,26] follow this schematization phenomenologically, introducing two sets of apparent diffusion coefficients and saturation concentrations to be constrained in experiments.

From a thermodynamic point of view, the key moment here is that the joint equilibrium concentrations of dissolved components in the solvent phase are determined by the composition of the oil phase in cells. Consider a special case of a two-component solute, when a transport zone of component S_1 overlaps with the core of component S_2. While the S_2 component distributed between two phases is in a local thermodynamic equilibrium, the chemical potential of component S_1 is influenced by the presence of the second component. This situation can only be described within the framework of a rigorous thermodynamic approach. Fick's law with constant concentration-independent tensor is not straightforwardly applicable to this problem.

The aim of the present work is to develop a sophisticated mathematical model of fatty oil extraction at SFE conditions within the framework of the SC approach. The model rigorously considers the internal resistance to the mass transfer of dissolved oil components along the inter-cell transport channels in the plant material and the multicomponent nature of the oil. The oil phase is presented as a "mechanical mixture" of two components. The size of TAG molecules prevents their self-diffusion and statistical mixing. Mathematically, neither excess terms nor statistical contributions to the thermodynamic potential are considered. Thus, equivalently, the oil phase is considered a set of two interpenetrating phases composed of different TAG species.

The solution, i.e., the solvent phase, is described as a regular solution with a pair-wise interaction parameter per pair of components in the mixture: three parameters, Ω_1, Ω_2, and Ω, are introduced. They are explained in Section 2.2. A limiting scenario of an ideal solution is considered as well and compared with the model based on the regular solution approach. The limiting case is considered when all three parameters tend to zero.

The Gibbs free energy is employed as a thermodynamic basis to define the equilibrium states and describe the co-existence conditions of phases.[27] Thus, the chemical potentials of solvent-phase components are straightforwardly obtained. The chemical potential, i.e., its spatial gradient, is the fundamental quantity used in the non-equilibrium thermodynamics[28] to describe the diffusion fluxes on the particle scale. Another quantity is the tensor of diffusion coefficients, which is a function of the local solution composition in isothermal−isobaric conditions of SFE. Finally, the constitutive relations of the mass fluxes of solution components with the chemical potential gradients are derived in the framework of the Stefan−Maxwell approach.[29−31] It is shown that the second component may act either as a co-solvent, facilitating the extraction rates of the first component, or as an anti-solvent decreasing the overall extraction rates. Finally, possible conditions of multiphase fluid flow existence on the packed bed scale are discussed.

2. THERMODYNAMIC EQUILIBRIA IN THE SYSTEM OIL + CO_2

2.1. The Oil Phase. The oil phase is considered a "mechanical mixture" of two pseudo-components designated as S_1 and S_2. From a thermodynamic point of view, this

https://doi.org/10.1021/acs.iecr.3c01488
Ind. Eng. Chem. Res. XXXX, XXX, XXX−XXX

assumes that any chemical interactions or statistical contributions to the Gibbs energy of the oil phase, as a whole, are neglected, and the oil is treated as a mixture of two interpenetrating phases of individual oil components, S_1 and S_2. Once one of these compounds is exhausted through dissolution and diffusion in the solvent phase, the oil becomes a remainder single-compound phase. The thermodynamic state of each pure component at extraction conditions (temperature T and pressure p) is considered its reference state.

Solvent molecules dissolve in the oil phase as well.[32] However, this fact is not well-studied and is typically ignored in SFE modeling. In the present article, the focus is on the description of the solution phase. It is assumed that the thermodynamic state of the oil phase $S_1 + S_2$ is not affected by the solvent molecules dissolved in it.

Accordingly, the Gibbs energy of $n_t^{(\mathrm{oil})} = n_1^{(\mathrm{oil})} + n_2^{(\mathrm{oil})}$ moles of the oil phase (see the Nomenclature section for definitions) at the chosen reference state is zero:

$$\frac{G^{(\mathrm{oil})}}{RT} = 0 \tag{1}$$

as well as the chemical potentials of each oil component S_i, i = 1, 2:

$$\frac{\mu_i^{(\mathrm{oil})}}{RT} = 0, \quad i = 1, 2$$

2.2. The Solvent Phase. The solvent (or solution) phase is a mixture of CO_2 molecules with a limited amount of two pseudo-components of oil, S_1 and S_2, dissolved in it. The supercritical extraction conditions of the solvent (pure CO_2) are the reference state for the solution, and $x_i^{(\mathrm{CO_2})} = n_i^{(\mathrm{CO_2})}/n_t^{(\mathrm{CO_2})}$, i = 1, 2, are the molar fractions of oil component S_i dissolved in the solvent phase, and $x_0^{(\mathrm{CO_2})} = n_0^{(\mathrm{CO_2})}/n_t^{(\mathrm{CO_2})} = 1 - x_1^{(\mathrm{CO_2})} - x_2^{(\mathrm{CO_2})}$ is the molar fraction of solvent molecules. The phase in a thermodynamically stable state exists only at a low content of dissolved oil components, $x_i^{(\mathrm{CO_2})} \to 0$, i = 1, 2. Otherwise, pure oil precipitates as a separate phase if $x_i^{(\mathrm{CO_2})}$ exceeds certain values, and the ternary system becomes heterogeneous.

2.2.1. Regular Solution Approach. First, let us consider a two-component system $S_i + CO_2$, assuming that the other oil component, $S_{j\neq i}$, is absent. A typical plot of the Gibbs energy of the $(S_i + CO_2)$ solution as a function of molar concentration $x_i^{(\mathrm{CO_2})}$ is shown in Figure 1 by the black curve at different Ω values (see the caption). The energy graphs have a parabolic form with their minimum at $\bar{x}_i^{0(\mathrm{CO_2})} < 0.2$.

The regular solution model (or Gibbs energy expansion) is aimed at representing the solid curve within the range where the phase is stable. Accordingly, the three-component system suggests the following expansion for the Gibbs energy of $n_t^{(\mathrm{CO_2})}$ moles of the solvent-phase molecules:

$x_i^{(\mathrm{CO_2})} \to 0$:

$$\frac{G^{(\mathrm{CO_2})}}{RT} = \overbrace{n_1^{(\mathrm{CO_2})} g_1^{(\mathrm{CO_2})} + n_2^{(\mathrm{CO_2})} g_2^{(\mathrm{CO_2})}}^{\text{reference state}} + \overbrace{n_1^{(\mathrm{CO_2})} \ln x_1^{(\mathrm{CO_2})} + n_2^{(\mathrm{CO_2})} \ln x_2^{(\mathrm{CO_2})} + n_0^{(\mathrm{CO_2})} \ln x_0^{(\mathrm{CO_2})}}^{\text{ideal mixing}} + \overbrace{n^{(\mathrm{CO_2})}(\Omega_1 x_1^{(\mathrm{CO_2})} x_0^{(\mathrm{CO_2})} + \Omega_2 x_2^{(\mathrm{CO_2})} x_0^{(\mathrm{CO_2})} + \Omega x_1^{(\mathrm{CO_2})} x_2^{(\mathrm{CO_2})})}^{\text{excess terms}} \tag{2}$$

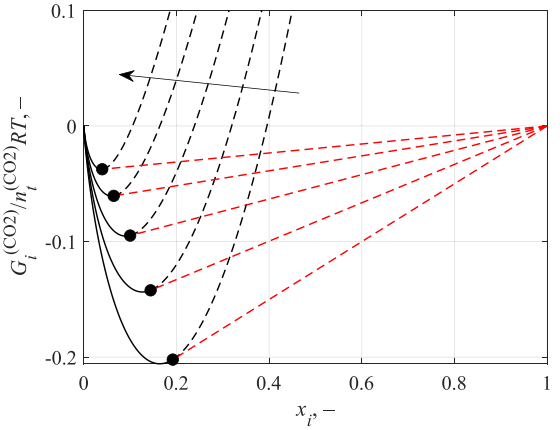

Figure 1. Schematic representation of the molar Gibbs energy of the two-component system $S_i + CO_2$ at $x_{j\neq i} = 0$, $g_i^{(\mathrm{CO_2})} = \ln 10$, and $\Omega_i = 0$. The arrow shows the increase of $\Omega = \{-1, -0.5, 0, 0.5, 1\}$. The black solid curve is the assumed approximation of the Gibbs energy of the solvent (solution) phase (eq 2), with only the S_i oil component dissolved in it.[33] The black point $x_i = \bar{x}_i^{0(\mathrm{CO_2})} < 0.2$ is the equilibrium solvent-phase composition. The red dashed line is a tie line representing the two-phase equilibrium of the solvent phase at $x_i = \bar{x}_i^{0(\mathrm{CO_2})} < 0.2$ and a single-component oil phase S_i, $x_i = 1$.

with

$$n_t^{(\mathrm{CO_2})} = n_1^{(\mathrm{CO_2})} + n_2^{(\mathrm{CO_2})} + n_0^{(\mathrm{CO_2})},$$
$$x_1^{(\mathrm{CO_2})} + x_2^{(\mathrm{CO_2})} + x_0^{(\mathrm{CO_2})} = 1$$

where the superscript (CO_2) refers to the solvent phase, Ω_i are the solvent$-S_i$ binary interaction parameters and Ω is the S_1-S_2 binary interaction parameter within the solvent medium. Finally, the transition energy $RTg_i^{(\mathrm{CO_2})}$ is the molar Gibbs energy that the oil molecule S_i gains upon transition from the oil phase (the reference state) to the solvent phase.

The corresponding chemical potentials of all three components at $x_i^{(\mathrm{CO_2})} < \bar{x}_i^{0(\mathrm{CO_2})}$ are expanded as follows as the partial derivatives of the Gibbs energy:

$$\frac{\mu_1^{(\mathrm{CO_2})}}{RT} \equiv \frac{1}{RT}\frac{\partial G^{(\mathrm{CO_2})}}{\partial n_1^{(\mathrm{CO_2})}} = g_1^{(\mathrm{CO_2})} + \ln x_1^{(\mathrm{CO_2})} + (1 - x_1^{(\mathrm{CO_2})})(\Omega_1 x_0^{(\mathrm{CO_2})} + \Omega x_2^{(\mathrm{CO_2})}) - \Omega_2 x_2^{(\mathrm{CO_2})} x_0^{(\mathrm{CO_2})} \tag{3}$$

$$\frac{\mu_2^{(\mathrm{CO_2})}}{RT} \equiv \frac{1}{RT}\frac{\partial G^{(\mathrm{CO_2})}}{\partial n_2^{(\mathrm{CO_2})}} = g_2^{(\mathrm{CO_2})} + \ln x_2^{(\mathrm{CO_2})} + (1 - x_2^{(\mathrm{CO_2})})(\Omega_2 x_0^{(\mathrm{CO_2})} + \Omega x_1^{(\mathrm{CO_2})}) - \Omega_1 x_1^{(\mathrm{CO_2})} x_0^{(\mathrm{CO_2})} \tag{4}$$

$$\frac{\mu_0^{(\mathrm{CO_2})}}{RT} \equiv \frac{1}{RT}\frac{\partial G^{(\mathrm{CO_2})}}{\partial n_0^{(\mathrm{CO_2})}} = \ln x_0^{(\mathrm{CO_2})} + (1 - x_0^{(\mathrm{CO_2})})(\Omega_1 x_1^{(\mathrm{CO_2})} + \Omega_2 x_2^{(\mathrm{CO_2})}) - \Omega x_1^{(\mathrm{CO_2})} x_2^{(\mathrm{CO_2})} \tag{5}$$

To simplify the following discussion, we set $\Omega_i = 0$ (if not stated explicitly) and consider various extraction regimes, characterized with different Ω values. This approach will be called the regular solution model at $\Omega \neq 0$.

https://doi.org/10.1021/acs.iecr.3c01488
Ind. Eng. Chem. Res. XXXX, XXX, XXX−XXX

2.2.2. The Limiting Case of an Ideal Solution. The above thermodynamic model given by eqs 2−5 can be further simplified in the ideal solution limit for the solvent phase at $\Omega \to 0$:

$$\frac{^{\text{ideal}}\mu_i^{(CO_2)}}{RT} = g_i^{(CO_2)} + \ln x_i^{(CO_2)}, \quad i = 0, 1, 2 \tag{6}$$

In this case, as shown in Section 3.5, the mass balance equations can be solved explicitly.

2.3. General Thermodynamic Phase Equilibria in the Ternary System. Depending on the overall composition of the three-component system, various sets of phases can co-exist in equilibrium at SFE conditions, i.e., (3) S_1 + S_2 + solution, (2) S_i + solution, or (1) solution. The corresponding phase diagram of the ternary system is shown in Figure 2. The

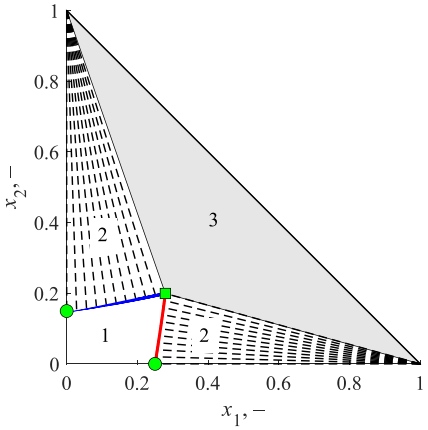

Figure 2. Phase diagram of the three-component system S_1 + S_2 + CO_2 with overall compositions corresponding to three (3), two (2), and single (1) phase equilibria at $g_i^{(CO_2)} = 1.6118$, $\Omega_1 = -\Omega_2 = -0.4$, and $\Omega = -1$. The horizontal axis is the overall mole fraction x_1 of the oil component S_1 in the system.[34] The vertical axis is the overall mole fraction x_2 of the oil component S_2 in the system. The gray triangle covers the overall compositions corresponding to the oil−solvent equilibrium S_1 + S_2 + CO_2. The red curve is the solvent-phase composition in equilibrium with the pure oil component S_1. The blue curve is the solvent-phase composition in equilibrium with the pure oil component S_2. The dashed lines are tie lines. Domain (1) represents the single phase of the solvent with dissolved oil components S_1 and S_2. The square marker is the joint equilibrium concentration at saturation $(\overline{x}_1^*, \overline{x}_2^*) = (0.2021, 0.0929)$ of the solvent phase in equilibrium with the S_1 + S_2 oil phase. The circles correspond to the equilibrium saturation concentrations $\overline{x}_1^0 = 0.25$ and $\overline{x}_2^0 = 0.15$ of solutes in the solvent phase in a two-component system (see eqs 7−12) when the other oil component is absent.

Gibbs energy of the solvent phase in region 1 is described by eq 2. Pure (two-phase, two-component) oil is represented by a line $x_1 + x_2 = 1$ and co-exists with the solution phase within region 3. The oil Gibbs energy is zero according to eq 1. The Gibbs energy of the two-phase system varies linearly along the tie (dashed) lines in region 2, and it is a plane in region 3.

The chemical potentials of the oil component S_i in different co-existing phases are equal. It is called diffusive (or material) equilibrium with respect to component S_i. The composition of the solvent phase in equilibrium with the corresponding oil component is shown with the blue (for S_2) and red (for S_1) curves in Figure 2. The equilibrium molar fractions of dissolved oil molecules in the solvent phase along the broken red-blue curve are designated as $x_i^{(CO_2)} = \overline{x}_i$, $i = 1, 2$. Finally, the red curve in Figure 2 is determined by

$$\mu_1^{(CO_2)}(\overline{x}_1, \overline{x}_2) = \mu_1^{(oil)} \equiv 0 \tag{7}$$

and the blue curve corresponds to

$$\mu_2^{(CO_2)}(\overline{x}_1, \overline{x}_2) = \mu_2^{(oil)} \equiv 0 \tag{8}$$

The three-phase equilibrium, i.e., the triangular region 3 in Figure 2, is described by the unique solvent-phase composition $x_1^{(CO_2)} = \overline{x}_1^*$ and $x_2^{(CO_2)} = \overline{x}_2^*$, while its two other vertices represent pure oil components (or phases) S_1 and S_2. The composition $(\overline{x}_1^*; \overline{x}_1^*)$ is the solution of simultaneous eqs 7 and 8. This point is shown by the square marker in Figure 2.

The interaction parameters Ω_i are one-to-one related to the saturation concentration $\overline{x}_i^0$ of oil component S_i in the solvent phase in the absence of another component $S_{j\neq i}$. These concentrations are shown by circles in Figure 2 and can be experimentally observed. In the limit of a two-component system, the respective (CO_2 + S_1) or (CO_2 + S_2) chemical potentials in eqs 3 and 4 reduce to

$$\frac{\mu_1^{(CO_2)}}{RT} = g_1^{(CO_2)} + \ln x_1^{(CO_2)} + \Omega_1(1 - x_1^{(CO_2)})^2, \quad x_2^{(CO_2)} = 0, \quad x_1^{(CO_2)} + x_0^{(CO_2)} = 1 \tag{9}$$

$$\frac{\mu_2^{(CO_2)}}{RT} = g_2^{(CO_2)} + \ln x_2^{(CO_2)} + \Omega_2(1 - x_2^{(CO_2)})^2, \quad x_1^{(CO_2)} = 0, \quad x_2^{(CO_2)} + x_0^{(CO_2)} = 1 \tag{10}$$

The saturation concentration $\overline{x}_i^0$ in the solvent phase corresponds to its equilibrium with the oil phase at the zero chemical potential $\mu_i^{(CO_2)}$ of the dissolved oil component S_i and in the absence of the other component $S_{j\neq i}$:

$$\mu_1^{(CO_2)}(\overline{x}_1 = \overline{x}_1^0, \overline{x}_2 = 0) = 0, \quad \mu_2^{(CO_2)}(\overline{x}_1 = 0, \overline{x}_2 = \overline{x}_2^0) = 0 \tag{11}$$

From eq 11 with the use of eq 9 or 10, we obtain

$$\Omega_i = -\frac{g_i^{(CO_2)} + \ln \overline{x}_i^0}{(1 - \overline{x}_i^0)^2}, \quad i = 1, 2 \tag{12}$$

Equations 12 relate the experimentally measurable quantities—equilibrium solution concentrations—with the transition energies $RTg_i^{(CO_2)}$ and interaction parameters Ω_i, $i = 1, 2$.

Once it is assumed that $\Omega_i = 0$, the equilibrium concentration of the solution component, directly follows from eqs 6 and 12:

$$\overline{x}_i^0 = \exp(-g_i^{(CO_2)}), \quad i = 1, 2$$

3. THREE-COMPONENT SC MODEL

3.1. Physical Description of the Model. Particles of ground seeds (the raw material) are the clusters of plant cells (1) and transport channels, i.e., intercellular channels (3), as shown in Figure 3.[35] The cells and the transport channels are separated by permeable cell membranes (6). The solvent phase with dissolved oil components occupies the transport channels. The oil phase is distributed in cells in the form of inclusions—oil bodies (4). The initial content of each pseudo-component, S_1 and S_2, of extractable oil compounds per unit volume of the

https://doi.org/10.1021/acs.iecr.3c01488
Ind. Eng. Chem. Res. XXXX, XXX, XXX−XXX

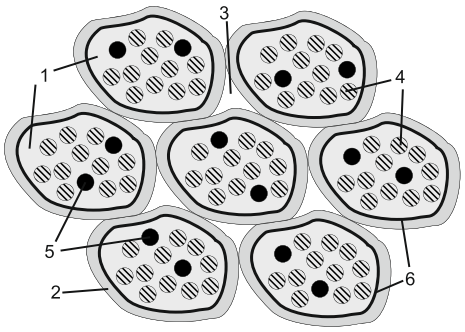

Figure 3. Schematics of oil distribution in cells and transport channels in a particle of ground raw material. (1), plant cell; (2), cell wall; (3), intercellular space; (4), oil bodies; (5), inclusions of indissoluble components; (6), permeable cell membrane.

raw material is designated as Θ_i, $i = 1, 2$. At a given temperature and pressure, the SFE process is governed by the limiting concentration pair $(\overline{x}_1^*, \overline{x}_2^*)$ of these compounds in the solvent phase at equilibrium with the oil phase.

The permeability of cell membranes and conductivity of transport channels control the rates of internal mass transfer in the raw material during SFE. The solvent, penetrating into the raw material, dissolves the oil molecules up to a particular saturation concentration $(\overline{x}_1, \overline{x}_2)$—the red-blue boundary of region 1 in Figure 2. The dissolved solute diffuses out of the cell across the cell membrane into the transport channels. Following the diffusion path under the gradient of chemical potential, the solute reaches the particle surface. The local solvent-phase composition $(\overline{x}_1, \overline{x}_2)$ depends on the oil phase composition and follows the broken red-blue curve in Figure 2. In the region of the particle where the oil exists only in a dissolved form, the composition of the solvent phase (x_1, x_2) is inside region 1; see Figure 2.

In the framework of the multicomponent shrinking core (MC-SC) model, it is assumed that Θ_i is relatively high for every oil component with respect to $\overline{\theta}_i^*$—the mass density of oil component S_i dissolved in the solvent in the extraction conditions, i.e., $\Theta_i \gg \overline{\theta}_i^*$, $i = 1, 2$. The resistance of the transport channels is the principal factor limiting the internal mass transfer.[14,23,36,37] Consequently, a local thermodynamic equilibrium between the oil in cells and the solvent in surrounding transport channels is reached instantaneously, and sharp concentration fronts form and move inside every particle of the raw material, as schematically shown in Figure 4. A single front exists per one oil pseudo-component.

For simplicity, flat (plain) particles of thickness $2a$ are considered in the research. The Cartesian coordinate z is introduced in every particle; $z = 0$ at the particle surface, and $z = a$ at the particle plane of symmetry. In a three-component system, two concentration fronts $z = as_1(t)$ and $z = as_2(t)$ can be distinguished. Assume $s_1 > s_2$. Three intervals, (1) shrinking core 1, $a > z > as_1$; (2) the overlap of shrinking core 2 and transport zone 1, $as_1 > z > as_2$; and (3) the transport zone 2, $as_2 > z > 0$, are distinguished. In the first interval, the oil phase is composed of all two components, and a three-phase equilibrium, $S_1 + S_2 + CO_2$, takes place. There is no diffusion in this region since $\mu_1^{(CO_2)} = \mu_2^{(CO_2)} \equiv 0$ at $z > as_1$, and the fixed solvent-phase composition $(\overline{x}_1^*, \overline{x}_2^*)$ is given by the square marker in Figure 2.

In interval (2), the oil phase is only presented by component S_2, and a two-phase equilibrium, $S_2 + CO_2$, is observed.

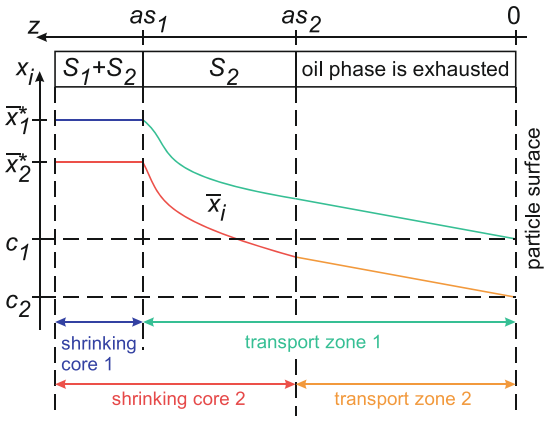

Figure 4. Schematics of the internal oil content distribution in a single particle of the ground raw material in cells and transport channels. The superscript (CO_2) is omitted. For every component, a corresponding pair of a transport zone and a core is labeled. The size of the transport zone is $z = as_1$ and $z = as_2$, respectively. The blue section of the x_1 distribution is in SC 1 and is solely governed by the phase equilibrium. The green section of x_1 distribution is in transport zone 1. Here, x_1 gradually decreases from $\overline{x}_1^*$ at the core boundary to the solvent concentration c_1 at the particle surface. The concentration profiles have a more complex structure in the region of SC 2 since it overlaps with transport zone 1. Therefore, $x_2 = \overline{x}_2(s_2) < x_2^*$ at the boundary of the transport zone 2.

However, the solvent phase is a solution of all three species since the species S_1 diffuses from the surface of SC 1 through interval (2) toward the particle surface. The local solute concentration $(\overline{x}_1, \overline{x}_2)$ in the solvent phase in $as_1 > z > as_2$ varies following the blue curve in Figure 2. Since the content of S_2 molecules dissolved in the solvent phase is governed by the equilibrium with the oil phase, one, thermodynamic, degree of freedom is fixed by $\mu_2^{(CO_2)} = 0$. Another degree of freedom remains. It is due to the non-equilibrium distribution of the dissolved oil component S_1, which is fixed by the differential mass balance equation (to be discussed in the following sections). Apparently, the instantaneous dissolution of the oil component S_2 in the solvent in the second interval and a limited solubility of oil components in the solvent phase influence the diffusion rates of both components. This process is considered and described in the next section by relating the diffusion coefficients to the chemical potentials of dissolved species in the solvent.

In the last interval, $as_2 > z > 0$, all two components of the oil phase are exhausted, and both degrees of freedom are fixed by the mass balance equations with the dependence of diffusion coefficients on the local composition of the solvent phase.

3.2. Typical Values of Model Parameters. The measurable quantities are conventionally given in terms of the mass densities of components. Among them, Θ_i is the initial mass per unit volume of the raw material, $\overline{\theta}_i^*$—the mass of oil component S_i per unit volume of the solvent phase in the extraction conditions in equilibrium with the oil phase. These quantities are directly related to the molar densities of components $n_j^{(CO_2)}$, $j = 0, 1, 2$.

By definition, the fluid density is

$$\rho_f = n_0^{(CO_2)} M_0$$

where $M_0 = 44$ g/mol is the molar mass of CO_2.

Similarly, we have

https://doi.org/10.1021/acs.iecr.3c01488
Ind. Eng. Chem. Res. XXXX, XXX, XXX−XXX

$$\overline{\theta}_i^* = n_i^{(CO_2)} M_i \equiv n_t^{(CO_2)} \overline{x}_i^* M_i$$

where $M_i \sim 850$ g/mol is the molar mass of the oil component S_i, $i = 1, 2$.

Typically, $n_i^{(CO_2)} \ll n_0^{(CO_2)} \approx n_t^{(CO_2)}$, and

$$\overline{\theta}_i^* \approx n_0^{(CO_2)} \overline{x}_i^* M_i = \overline{x}_i^* \frac{M_i}{M_0} \rho_f \tag{13}$$

Thus, the constraint for the MC-SC applicability can be rewritten in terms of molar concentrations:

$$\Theta_i \gg \overline{x}_i^* \frac{M_i}{M_0} \rho_f$$

To estimate the equilibrium molar concentrations $(\overline{x}_1^*, \overline{x}_2^*)$ from eq 13, one obtains

$$\overline{x}_i^* \approx \frac{\overline{\theta}_i^*}{\rho_f} \frac{M_0}{M_i}$$

Consequently, assuming $M_0 = 44$ g/mol, $M_i = 850$ g/mol, $\rho_f = 700$ kg/m^3, and $\overline{\theta}_i^* = 15$ kg/m^3, one arrives at typical values of $\overline{x}_i^*$ and $\overline{x}_i^0$ on the order of 10^{-3}.

3.3. Stefan−Maxwell Approach for Diffusion Fluxes.

In this section, the superscript (CO_2) is omitted, since all the derivations are related to the solvent phase and the diffusion in it. Let n_j, $j = 0, 1, 2$, be the molar density of component j in the solvent phase. The total molar density of the solvent phase is $n_t = n_0 + n_1 + n_2$. The molar flux N_j of the jth species with respect to a particle-fixed coordinate reference frame is given by

$$N_j = n_j u_j = x_j N_t + X_j, \quad N_t = N_0 + N_1 + N_2, \quad j = 0, 1, 2 \tag{14}$$

where X_j is the molar diffusion flux of species j relative to the molar average reference velocity u,

$$N_t \equiv n_t u = n_0 u_0 + n_1 u_1 + n_2 u_2$$

of the multicomponent solvent phase in the z direction, and u_j is the velocity of the diffusing species. All fluxes and velocities are related to the overall cross-sectional area, which passes through the cells as well as the channels.

The multicomponent diffusion affected by the local multiphase thermodynamic equilibrium is modeled in the framework of the Stefan−Maxwell approach.[30,38,39] To derive the equations for diffusion fluxes, let us consider species 1 first. The driving force $-\mathrm{d}\mu_1/\mathrm{d}z$ for transport in the positive z direction is balanced by the friction between species 1 and other two species, 0 and 2, in the system. We may expect that the frictional drag between species, i.e., 1 and 2, will be proportional to the difference of velocities $(u_1 - u_2)$ and to the concentration of the mixture, i.e., the mole fraction x_2 of component 2. Considering that two drag forces are exerted on each species in a three-component system

$$-\frac{\mathrm{d}\mu_1}{\mathrm{d}z} = x_0 \frac{u_1 - u_0}{\mathcal{D}_{01}/RT} + x_2 \frac{u_1 - u_2}{\mathcal{D}_{12}/RT} \tag{15}$$

and multiplying force balance eq 15 for species 1 by x_1/RT, one obtains

$$-\frac{x_1}{RT}\frac{\mathrm{d}\mu_1}{\mathrm{d}z} = \frac{x_0 x_1 u_1 - x_1 x_0 u_0}{\mathcal{D}_{01}} + \frac{x_2 x_1 u_1 - x_1 x_2 u_2}{\mathcal{D}_{12}} \tag{16}$$

where the factor $RT/\mathcal{D}_{ij}$ may be interpreted to be the drag coefficient between species i and j. The coefficients $\mathcal{D}_{ij}$ are apparent ones and proportional to the volume fraction of transport channels.[24,40]

The set of definitions in eq 14 and $n_j = x_j n_t$ as well as a straightforward relation

$$x_i N_j - x_j N_i = x_i X_j - x_j X_i$$

allow rewriting eq 16 in terms of molar diffusion fluxes:

$$d_1 \equiv -\frac{x_1}{RT}\frac{\mathrm{d}\mu_1}{\mathrm{d}z} = \frac{x_0 X_1 - x_1 X_0}{n_t \mathcal{D}_{01}} + \frac{x_2 X_1 - x_1 X_2}{n_t \mathcal{D}_{21}} \tag{17}$$

The force balance for the other two species yields

$$d_0 \equiv -\frac{x_0}{RT}\frac{\mathrm{d}\mu_0}{\mathrm{d}z} = \frac{x_1 X_0 - x_0 X_1}{n_t \mathcal{D}_{10}} + \frac{x_2 X_0 - x_0 X_2}{n_t \mathcal{D}_{20}} \tag{18}$$

$$d_2 \equiv -\frac{x_2}{RT}\frac{\mathrm{d}\mu_2}{\mathrm{d}z} = \frac{x_0 X_2 - x_2 X_0}{n_t \mathcal{D}_{02}} + \frac{x_1 X_2 - x_2 X_1}{n_t \mathcal{D}_{12}} \tag{19}$$

Equations 17−19 are formulated in terms of molar diffusion fluxes X_j, $j = 0, 1, 2$. However, they are linearly dependent and determine only the relative motion of the mixture components. An additional constraint should be imposed to fix the degrees of freedom, associated with the overall motion of the mixture due to the diffusion process.

With this in mind, let us consider the mass densities of the two interchanging phases in the system. The densities of oil and the solvent are very close at SFE conditions and equal to ∼700 to 800 kg/m^3, and replacement of the oil phase with the solvent phase occurs at a practically constant mass density. The overall mass flux of the components in the system is zero:

$$J_0 + J_{12} = 0, \quad J_{12} \equiv J_1 + J_2 \tag{20}$$

where

$$J_j = M_j X_j, \quad j = 0, 1, 2 \tag{21}$$

are the mass diffusion fluxes.

Combining eqs 21 and 20, we get

$$X_0 = -\frac{M_1}{M_0} X_1 - \frac{M_2}{M_0} X_2$$

and after substitution of X_0 into eqs 17 and 19, we arrive at driving forces d_i:

$$d_1 \equiv -\frac{x_1}{RT}\frac{\mathrm{d}\mu_1}{\mathrm{d}z} = \frac{\left(x_0 + \frac{M_1}{M_0} x_1\right) X_1 + x_1 \frac{M_2}{M_0} X_2}{n_t \mathcal{D}_{01}} + \frac{x_2 X_1 - x_1 X_2}{n_t \mathcal{D}_{21}} \tag{22}$$

$$d_2 \equiv -\frac{x_2}{RT}\frac{\mathrm{d}\mu_2}{\mathrm{d}z} = \frac{\left(x_0 + x_2 \frac{M_2}{M_0}\right) X_2 + x_2 \frac{M_1}{M_0} X_1}{n_t \mathcal{D}_{02}} + \frac{x_1 X_2 - x_2 X_1}{n_t \mathcal{D}_{12}} \tag{23}$$

Equations 22 and 23 can be rewritten in a matrix form:

$$n_t d = BX, \quad d = \begin{pmatrix} d_1 \\ d_2 \end{pmatrix}, \quad X = \begin{pmatrix} X_1 \\ X_2 \end{pmatrix}$$

https://doi.org/10.1021/acs.iecr.3c01488
Ind. Eng. Chem. Res. XXXX, XXX, XXX−XXX

where

$$B \equiv \begin{pmatrix} B_{11} & B_{12} \\ B_{21} & B_{22} \end{pmatrix} = \begin{pmatrix} \frac{M_1}{M_0}\frac{x_1}{Đ_{01}} + \left(\frac{x_0}{Đ_{01}} + \frac{x_2}{Đ_{21}}\right) & -x_1\left(\frac{1}{Đ_{21}} - \frac{1}{Đ_{01}}\frac{M_2}{M_0}\right) \\ -x_2\left(\frac{1}{Đ_{12}} - \frac{1}{Đ_{02}}\frac{M_2}{M_0}\right) & \frac{x_2}{Đ_{02}} + \left(\frac{x_0}{Đ_{02}} + \frac{x_1}{Đ_{12}}\right)\frac{M_1}{M_0} \end{pmatrix}$$

To relate the Stefan−Maxwell approach with Fick's law, Fick's diffusion coefficient, $D = B^{-1}\Gamma/RT$, and the gradient of molar concentrations, $\partial x_i/\partial z$, the vector d should be given in terms of thermodynamic factor matrix—tensor Γ of chemical potential derivatives:[41,42]

$$d = -\frac{\Gamma}{RT}\begin{pmatrix} \frac{\partial x_1}{\partial z} \\ \frac{\partial x_2}{\partial z} \end{pmatrix}, \qquad \Gamma = \begin{pmatrix} x_1\frac{\partial \mu_1}{\partial x_1} & x_1\frac{\partial \mu_1}{\partial x_2} \\ x_2\frac{\partial \mu_2}{\partial x_1} & x_2\frac{\partial \mu_2}{\partial x_2} \end{pmatrix}$$

Hence, the Stefan−Maxwell approach suggests the factorization of Fick's diffusion coefficient, and distinguishing between the drag and the chemical (non-ideality) interactions between species becomes possible. The drag is described by the factor B^{-1}, while Γ controls the system non-ideality. In the simplest scenario, in the ideal system, $\Gamma = RT$, and Fick's diffusion tensor is $D = B^{-1}$. Thus, the tensor B accounts for the species concentrations in the solvent phase and disparity of different species molecules.

Finally, the vector $J = (J_1; J_2)$ of the mass diffusion fluxes is related to the molar concentration gradients as follows:

$$J = -n_t\frac{MB^{-1}\Gamma}{RT}\begin{pmatrix} \frac{\partial x_1}{\partial z} \\ \frac{\partial x_2}{\partial z} \end{pmatrix}, \qquad M = \begin{pmatrix} M_1 & 0 \\ 0 & M_2 \end{pmatrix} \tag{24}$$

Using eq 20, it is also possible to calculate the mass diffusion flux of the solvent, $J_0 = -J_{12}$, opposite with respect to the net oil flux $J_{12} = J_1 + J_2$.

3.4. Particle-Scale Mass Balance Equations and Model Assumptions. The maximum solute concentration, $\overline{x}_i^*$, in the solvent phase at supercritical conditions remains small. Thus, assuming $x_0 \approx 1$, $x_1 \approx 0$, and $x_2 \approx 0$, one can hereinafter consider the case of infinitely low dilution with a simplified expression for the matrix B:

$$B^{-1} \approx \begin{pmatrix} Đ_{01} & 0 \\ 0 & Đ_{02} \end{pmatrix} \tag{25}$$

Thus, $Đ_{0i}$, $i = 1, 2$, is interpreted as the apparent binary diffusion coefficient at infinitely low dilution of species 1 or 2 in the solvent (species 0) in transport channels of the raw material. The simplified form of matrix B, eq 25, reduces two parameters, $Đ_{12}$ and $Đ_{21}$, in the problem.

The low dilution level of oil components in the supercritical fluid is typical of the SFE process. Thus, it is assumed that $n_t \approx n_0 = \text{const}$.

Finally, the mass diffusion fluxes in eq 24 reduce to the following simplified form:

$$J_i = -Đ_{0i}n_0M_ix_i\frac{\partial}{\partial z}\left(\frac{\mu_i}{RT}\right), \qquad i = 1, 2 \tag{26}$$

or, equally, calculating the derivative in eq 26, we arrive at

$$J_i = -Đ_{0i}n_0M_i\frac{x_i}{RT}\left(\frac{\partial \mu_i}{\partial x_1}\frac{dx_1}{dz} + \frac{\partial \mu_i}{\partial x_2}\frac{dx_2}{dz}\right), \qquad i = 1, 2$$

Within the framework of the MC-SC model, the spatial distributions of dissolved oil concentrations in the channels of the corresponding transport zones are assumed to be quasi-stationary at any moment t,[43] i.e.,

$$as_i > z > 0: \qquad \frac{\partial J_i}{\partial z} = 0, \qquad i = 1, 2 \tag{27}$$

Thus, the fluxes of both oil components remain spatially constant and vary in time only, $J_i = J_i(t)$, $i = 1, 2$.

Importantly, this uniquely predetermines the concentration profiles in the region where SC 2 and transport zone 1 overlap, $as_1 > z > as_2$. The local composition of the solvent phase is fully determined by the diffusion of the dissolved component S_1 at material equilibrium with respect to the oil component S_2. This constraint is described in the framework of the Stefan−Maxwell approach.

There is a material equilibrium with respect to component S_2 in the overlap region. Here, the local composition can be predicted explicitly:

$$\mu_2(x_1, x_2) \equiv 0, \qquad as_1 > z > as_2$$

This equation agrees with eq 27 and assumes that the diffusion flux $J_2 \sim d\mu_2/dz$ of the second component is zero at $as_1 > z > as_2$, while $J_2 > 0$ at $z < as_2$ and $J_1 > 0$ at $z < as_1$. Thus, there exists a jump in J_i at $z = as_i$, $i = 1, 2$, related to the rate of ith core shrinking.

Finally, the problem that governs the overall spatial distributions of x_1 and x_2 in the flat particle for every oil component can be formulated explicitly as

$$as_1 > z > 0: \qquad \frac{\partial J_1}{\partial z} = 0 \tag{28}$$

$$as_1 > z > as_2: \quad \mu_2(x_1, x_2) \equiv 0; \qquad as_2 > z > 0: \quad \frac{\partial J_2}{\partial z} = 0 \tag{29}$$

The corresponding boundary conditions are

$$x_i|_{z=as_i} = \overline{x}_i^*, \qquad x_i|_{z=0} = c_i \tag{30}$$

where c_i is the molar fraction of oil component S_i at the particle boundary, in the surrounding bulk solution. These quantities are determined by the extractor-scale mass balance equations.

Once the so-called free oil is exhausted,[44,45] the concentration of the surrounding bulk solution becomes relatively low, and only the extraction of oil from large particles takes place. Outlet solute concentrations are 1−2 orders of magnitude smaller than the saturation concentration, and the bulk solution concentration becomes vanishingly small to affect

https://doi.org/10.1021/acs.iecr.3c01488
Ind. Eng. Chem. Res. XXXX, XXX, XXX−XXX

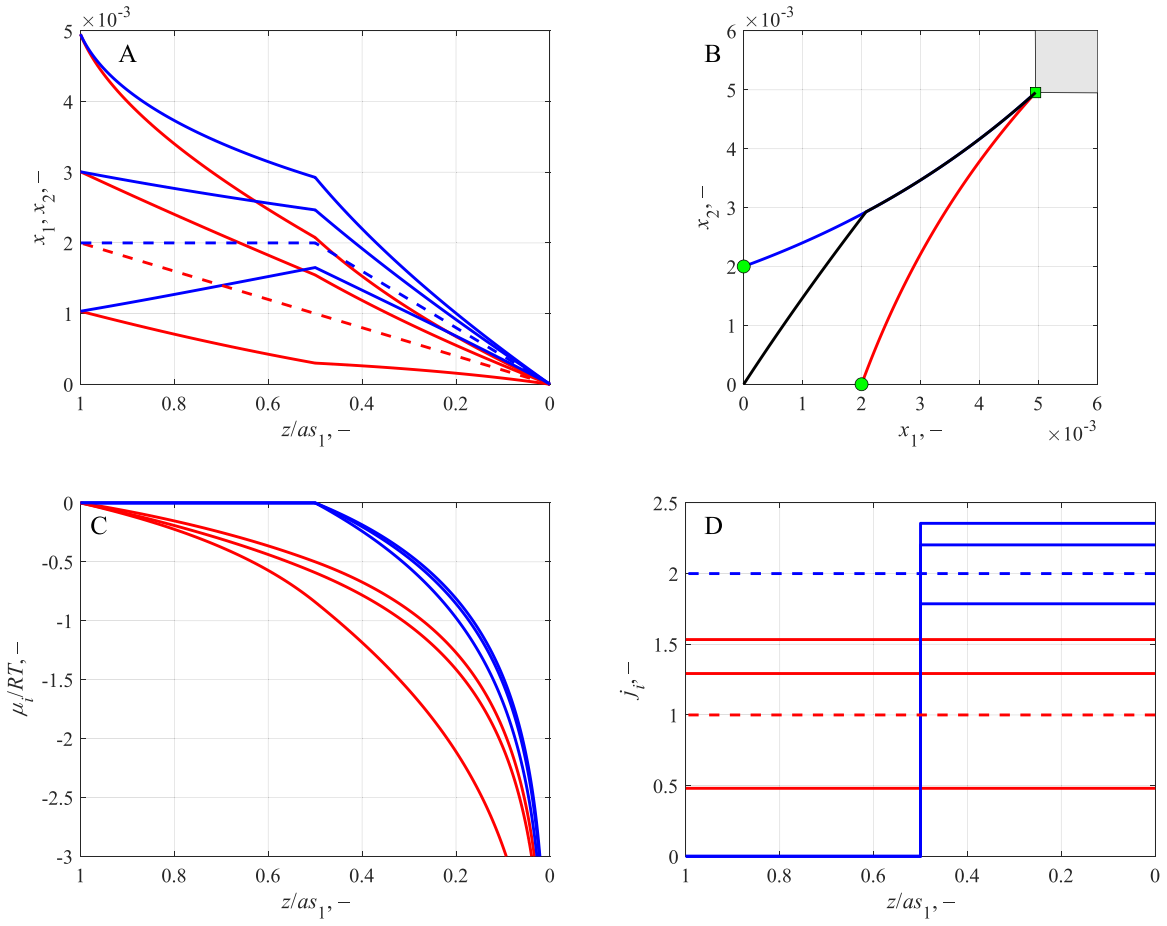

Figure 5. (A) Particle scale solute concentration distribution in the transport channels outside the inner SC 1, $z/as_1 < 1$, during extraction. Red curves, $x_1(z)$; blue curves, $x_2(z)$. The dashed curves correspond to the ideal solution model, eqs 6, 33, and 35, the solid curves − general, regular solution approach, eqs 26−31. The saturation concentrations are $\overline{x}_i^0 = 2 \times 10^{-3}$ and $s_2/s_1 = 0.5$. Solute interaction parameters from top to bottom $\Omega = \{-164.5, -120, 0, 440\}$. (B) Phase diagram of the three-component mixture at $\Omega = -164.5$. Blue curve, solvent-phase composition at equilibrium with the oil component S_2; red curve, solvent-phase composition at equilibrium with the oil component S_1. The gray polygon is the three-phase equilibrium domain. The black curve is the parametric plot of $\{x_1(z); x_2(z)\}$ distributions from panel (A). Each curve has two segments. The first segment follows the blue curve and corresponds to the interval $s_2/s_1 \le z/as_1 \le 1$ inside the particle. The second segment is inside the single-phase equilibrium domain. So, it corresponds to the outer transport zone interval $0 \le z/as_1 \le s_2/s_1$. (C) Chemical potential distributions corresponding to the plots in panel (A). (D) Dimensionless flux j_i, $i = 1, 2$, as a function of position within a particle. The definition of dimensionless flux j_i is given by eq 36.

the particle-scale extraction rates. To simplify further analysis and to ensure the numerical accuracy of the model equation solution, we consider vanishingly small solute concentrations on the macro-scale level of the packed bed, $c_i \sim 10^{-6} \ll \overline{x}_i^*$, $i = 1, 2$.

The problem in eqs 26−30 for $x_i(z, t, s_1, s_2)$ with μ_i given by eqs 3 and 4 for the regular solution model or eq 6 for the ideal solution limit can be solved in a closed form at any fixed values s_1 and s_2. Once the concentration distribution is obtained, one can calculate the flux $J_i(s_1, s_2)$, $i = 1, 2$, taking the gradient of x_i.

Another couple of equations relate the diffusion fluxes J_i with the rates of core shrinking, $\partial s_i/\partial t$. Let us consider the mass balance at the core boundaries, $z = as_i$, where the shrinking rates are balanced by the diffusion fluxes J_i:

$$\Theta_i a \frac{\partial s_i}{\partial t} = J_i(s_1, s_2) \equiv \mathcal{D}_{0i}\theta_i \frac{\partial}{\partial z}\left(\frac{\mu_i}{RT}\right), \quad i = 1, 2 \tag{31}$$

Here, $\theta_i = x_i n_0 M_i \le \theta_i^*$ is the mass density of oil component S_i dissolved in the solvent phase in the transport channels.

The coupled system of eqs 26−31 governs the particle-scale mass transfer in the framework of the two-component SC approach.

3.5. Ideal Solution Approach. A special limiting case, i.e., $\Omega_1 = \Omega_2 = \Omega = 0$, of a regular solution model is an ideal approach. The corresponding thermodynamic relations for chemical potentials are given by eq 6. The overall SFE model based on these simplified relations, which ignore any pairwise interactions of molecules in the solution, has been introduced earlier[25] and applied in ref 26 to modeling the selective extraction of phosphatidylcholine. The approach allows for the closed-form solution of model equations and can be considered a reference for the more sophisticated cases, when the species interactions are taken into account.

Substituting eq 6 into eq 26, calculating the partial derivatives $\partial\mu_i/\partial z$, and introducing the mass density of the solute components,

$$\theta_i = n_0 x_i M_i$$

we obtain the overall solute flux per unit area of particle surface:

https://doi.org/10.1021/acs.iecr.3c01488
Ind. Eng. Chem. Res. XXXX, XXX, XXX−XXX

$$J_i^{id} = -Đ_{0i}\frac{\partial \theta_i}{\partial z}, \qquad J_{12}^{id} = J_1^{id} + J_2^{id} \tag{32}$$

Equation 32 is Fick's law with the diffusion coefficients of species equal to the respective Stefan−Maxwell parameters $Đ_{0i}$.

The analytical expression for the flux in eq 32 can be derived explicitly.[36] In the simplified approach, the diffusion of every species is independent of the other component concentration, particularly, $\overline{x}_i^* = \overline{x}_i^0$, and a linear concentration distribution sets on in the transport zone of flat particles:

$$x_i = \overline{x}_i^0, \quad z = as_i; \quad x_i = c_i, \quad z = 0$$

$$\frac{\partial \theta_i}{\partial z} = n_0 M_i \frac{\overline{x}_i^0 - c_i}{as_i} \tag{33}$$

The solute concentration is constant, $x_i = \overline{x}_i^0$, in the ith shrinking core.

After substitution of eq 33 into eq 32, one arrives at

$$J_{12}^{id} = -n_0 Đ_{01} M_1 \frac{\overline{x}_1^0 - c_1}{as_1}\left(1 + \frac{s_1}{s_2}\frac{Đ_{02}M_2}{Đ_{01}M_1}\frac{\overline{x}_2^0 - c_2}{\overline{x}_1^0 - c_1}\right) \tag{34}$$

Hereinafter, in further consideration, we assume $Đ_{01} = Đ_{02} = Đ$, $M_1 = M_2 = M$, and $\overline{x}_1^0 = \overline{x}_2^0 = \overline{x}^0$ and neglect c_1 and c_2 compared to $\overline{x}_i^0$ and reduce eq 34 to

$$J_{12}^{sc} = -Đ\frac{\overline{\theta}^0}{as_1}\left(1 + \frac{s_1}{s_2}\right), \quad J_i^{sc} = Đ\frac{\overline{\theta}^0}{as_i}, \quad \overline{\theta}^0 = \overline{x}^0 n_0 M \tag{35}$$

Finally, the simplified relations in eq 35 can be compared to the overall flux

$$J_{12} = -Đ\left(\theta_1\frac{\partial}{\partial z}\left(\frac{\mu_1}{RT}\right) + \theta_2\frac{\partial}{\partial z}\left(\frac{\mu_2}{RT}\right)\right), \quad \theta_i = Mn_0x_i$$

predicted in the case of chemical interactions between species in the solvent phase. Accordingly, the scaled fluxes become

$$j_i = -as_1\frac{x_i}{\overline{x}^0}\frac{\partial}{\partial z}\left(\frac{\mu_i}{RT}\right) \equiv J_i\frac{as_1}{Đ\overline{\theta}^0}, \quad i = 1, 2 \tag{36}$$

$$j_{12} = -as_1\left(\frac{x_1}{\overline{x}^0}\frac{\partial}{\partial z}\left(\frac{\mu_1}{RT}\right) + \frac{x_2}{\overline{x}^0}\frac{\partial}{\partial z}\left(\frac{\mu_2}{RT}\right)\right) \equiv J_{12}\frac{as_1}{Đ\overline{\theta}^0}$$

3.6. Solute Concentration in the Pores of the Packed Bed.

Two different pairs of time scales typical of the SFE process can be introduced.[24,40] The first pair is associated with the time required for the depletion of component S_i in a particle of half-thickness a:

$$t_{sc}^{(1)} \sim \frac{\Theta_i}{\overline{\theta}_i^0}\frac{a^2}{Đ_{0i}}, \quad i = 1, 2$$

On the other hand, the fluid flowing through the packed bed tends to reach the saturation concentration $\overline{\theta}_i^0$. The saturation is attained for a particular component i within a typical time

$$t_{sc}^{(2)} \sim \frac{a^2 s_i}{Đ_{0i}}, \quad i = 1, 2$$

In the framework of a high initial oil content, the inequality $t_{sc}^{(1)} \gg t_{sc}^{(2)}$ is true. So, the transport zone thickness s_i cannot change significantly, while the solution concentration c_i increases from 0 to $\overline{x}_i^0$.

Finally, one can study the evolution of the solute concentration in the pores of the packed bed in the framework of fixed value of s_i, and the equation for the local concentration in the pores of the packed bed takes the following form:

$$\theta_i = n_0 M_i c_i = \frac{1-\varepsilon}{\varepsilon}\frac{3}{a}\int_0^t J_i(\varsigma)\, d\varsigma$$

with the dimensionless time

$$\tau = t/\frac{a^2 s_i}{Đ_{0i}}.$$

4. DISCUSSION

4.1. Particle-Scale Solute Concentrations. The particle-scale solute concentration distribution in the transport channels is non-monotonous and significantly non-linear and depends on the solute interaction parameter Ω, as demonstrated in Figure 5. Here, the solid curves correspond to the regular solution approach, eqs 26−31, which is compared with the ideal solution approach described by eqs 6, 33, and 35 and shown by the dashed curves.

The composition of the solvent phase in transport channels is given by the two molar concentrations of solute components, $x_1(z)$ and $x_2(z)$, which are strongly interrelated in the framework of the regular solution approach. The particular distributions $x_1(z)$ and $x_2(z)$ are determined by the time-dependent quantities s_2/s_1, c_1, and c_2, and, in the regular solution, by the fixed triple of solute interaction parameters, Ω_1, Ω_2, and Ω. The two parameters, $\Omega_i = 6.2395$, $i = 1, 2$, are set equal in Figure 5 and fixed so that the pairwise $S_i + CO_2$ molar saturation concentrations are $\overline{x}_i^0 = 2 \times 10^{-3}$. Other quantities are set as $s_2 = 0.5s$ and $c_1 = c_2 = 10^{-6} \ll \overline{x}_i^0$. The values of the third thermodynamic parameter, Ω, are given in the caption to Figure 5.

Inside of the inner SC 1, $z/as_1 > 1$, the three-phase equilibrium $CO_2 + S_1 + S_2$ sets on. So, $x_2 = \overline{x}_2^*$ and $x_1 = \overline{x}_1^*$ take constant values with respect to z. These values vary with Ω. The state of equilibrium is shown by the square marker, i.e., region 3, in the phase diagram in Figure 2 and in Figure 5B.

The quasi-stationary distributions of solute concentrations in the transport channels take place outside the innermost core 1, $1 > z/as_1 > 0$. This interval is covered by panels A, B, and C in Figure 5. Here, a material equilibrium with respect to the oil component S_2 is observed in the cells, and two sub-intervals, (1) $1 > z/as_1 > s_2/s_1$ and (2) $s_2/s_1 > z/as_1 > 0$, can be distinguished. They are separated by the outer SC surface 2 at $z = as_2$. The oil phase is still present in the first interval as a pure S_2 component, while the phase is absent from the second interval. Thus, the $x_2(z)$ dependence bends sharply at the outer SC surface, $z = as_2$; see Figure 5. This sharp bend appears in Figure 5B as well at the point where the black curve moves aside from the blue one.

In the first sub-interval, $1 > z/as_1 > s_2/s_1$, the composition of the solvent phase corresponds to the two-phase equilibria. These equilibria are shown by the blue curve in Figure 2 (as a general example) and in Figure 5B for a particular $\Omega = -164.5$. Along this curve, the chemical potential $\mu_1(x_1, x_2)$ decreases, taking its maximum value at $(\overline{x}_1^*; \overline{x}_2^*)$, while the chemical potential $\mu_2(x_1, x_2) \equiv 0$. Thus, only the diffusion of oil component 1 takes place in the "two-component" medium composed of the solvent with dissolved oil component S_2. The diffusion takes place in the direction opposite to the chemical

https://doi.org/10.1021/acs.iecr.3c01488
Ind. Eng. Chem. Res. XXXX, XXX, XXX−XXX

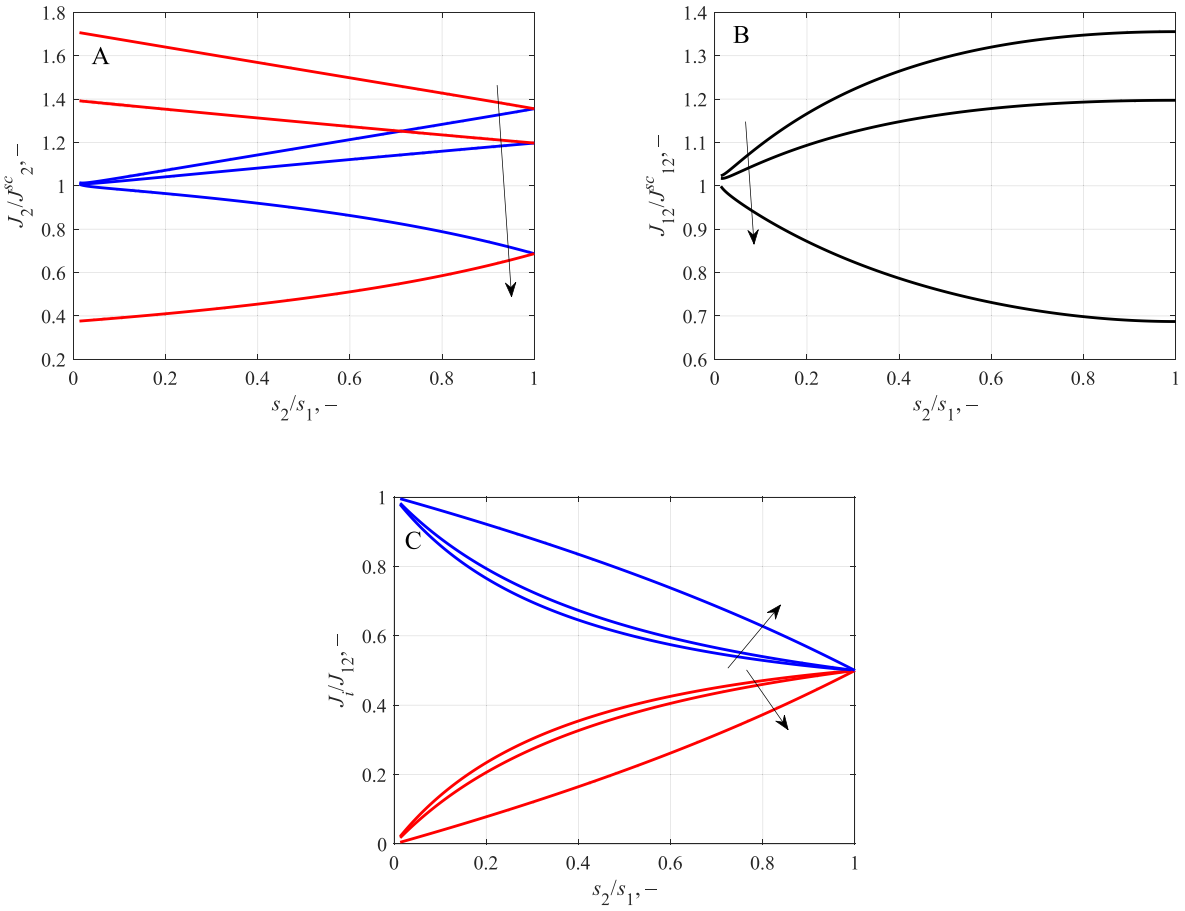

Figure 6. (A) The fluxes of S_1 (the red curves) and S_2 (the blue curves) oil components and (B) the overall flux J_{12} as functions of the outer transport zone size, s_2/s_1. (C) Fraction of the individual flux component in the overall flux. The model parameters are fixed at the same values as in Figure 5. The arrows show the direction of increase in $\Omega = \{-184, -136{,}640\}$.

potential gradient, as prescribed by the physical laws. This suggests that x_1 monotonically decreases toward the particle surface. The oil component S_2 responds to the diffusion of component S_1 by phase transition. Once x_2 exceeds the $\overline{x}_2$ value, the solution becomes oversaturated with respect to oil component S_2. Thus, its molecules form dispersed nuclei of the oil phase and precipitate from the solution phase to restore the equilibrium solvent-phase composition, i.e., $\mu_2(x_1, x_2) \equiv 0$. The flux of the second component is zero in $1 > z/as_1 > s_2/s_1$. The unidirectional diffusion of both oil components takes place in the second sub-interval, $as_2 > z$.

The $x_2(z)$ distributions shown by the blue curves in Figure 5A demonstrate different patterns in the region $1 > z/as_1 > s_2/s_1$, depending on the interaction scenario of S_1 and S_2 oil components within the solvent medium. The scenario could be either a co-solvent or an anti-solvent. The scenarios are typical attributes of the regular solution approach and cannot be described in the framework of the ideal solution limit, when $\overline{x}_i = \overline{x}_i^*$ is constant along the respective (red or blue) curve in the phase diagram.

The co-solvent scenario is observed for $\overline{x}_i^0 < \overline{x}_i^*$ at the equilibrium solubility $\overline{x}_i$ positively correlating with the other solubility $\overline{x}_{j \neq i}$ along the curve representing the solvent-phase concentrations in the phase diagram(Figure 5B). For the system configuration under consideration, it is at $\Omega < 0$, and $x_2(z)$ decreases toward the outer SC surface, and vice versa, in the anti-solvent scenario, $\overline{x}_i^0 > \overline{x}_i^*$, the two equilibrium concentrations $\overline{x}_1$ and $\overline{x}_2$ are negatively correlated at $\Omega > 0$, and $x_2(z)$ increases toward the core surface.

Finally, x_1 and x_2 tend at the SC 2 surface, $z = as_2$, to the values marked by circular markers in Figure 2. Thus, $x_2(z = as_2) \to \overline{x}_2^0$, and $x_1(z = as_2) \to 0$. However, this composition is typically not attained within the first subinterval outside the inner SC, $as_1 > z > as_2$. The boundary concentrations, $x_i(z = as_2)$, deviate from their respective limiting values.

In the second sub-interval, $as_2 > z > 0$, there is diffusion of both solute components under the chemical potential gradient, which is not affected by the local thermodynamic equilibrium with the oil phase. The phase is exhausted in this sub-interval. Both chemical potentials, μ_1 and μ_2, decrease toward the particle surface, leading to a constant mass flux along the z coordinate. Typically, the x_1 and x_2 distributions decrease monotonously toward the particle surface where vanishingly small solute concentrations are assumed, $c_i \to 0$.

Compare the described local solvent-phase composition with the composition obtained in the framework of the ideal solution approach, eqs 6 and 32−35. In the latter case, the diffusion follows Fick's law and any interactions between solute components in the solvent phase are neglected. The respective distributions of solute concentration are shown in Figure 5A by dashed curves. In the transport zones, $as_2 > z$ for the blue curve and $as_1 > z$ for the red curve, the solute concentrations vary linearly, while they remain constant within the respective SCs. The model based on the regular solution approach is

https://doi.org/10.1021/acs.iecr.3c01488
Ind. Eng. Chem. Res. XXXX, XXX, XXX−XXX

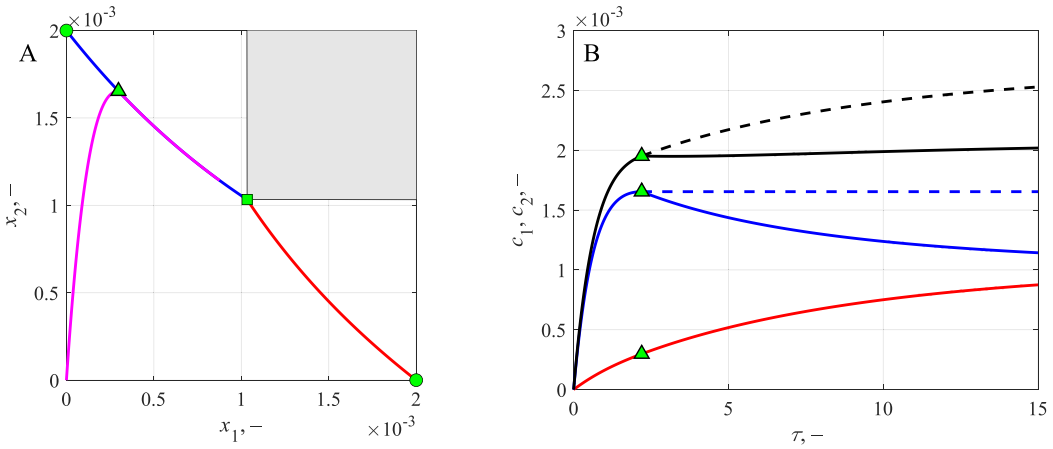

Figure 7. (A) Phase diagram of the three-component system. The magenta curve shows the trajectory of the solvent-phase composition $\{c_1; c_2\}$. (B) Solvent-phase solute concentration as a function of dimensionless time. The figure demonstrates the rates of solute accumulation in the pores of the packed bed while the solvent passes along the raw material particles. The red solid curve is $c_1(\tau)$, the blue solid curve is $c_2(\tau)$, and the black solid curve is the overall concentration $c_1 + c_2$. The dashed curves show the overall molar concentrations in the multiphase fluid.

significantly non-linear. Thus, the detailed particle-scale solute distribution is poorly approximated in the framework of the simplified approach.

Therefore, the solute flux at the particle surface—which is governed by the particle-scale solute concentration distribution—has to be carefully examined as well.

4.2. Oil Flux at the Particle Surface. There are two fluxes J_1 and J_2 of individual components as well as the overall oil phase flux, $J_{12} = J_1 + J_2$, in the two-component model of solute. The ratios between these three fluxes and the corresponding values predicted by the simplified (ideal solution) model, eqs 32−35, are shown in Figure 6 versus relative size s_2/s_1 of outer transport zone for different Ω values. The other input model parameters are same as in Figure 5.

The plots in Figure 6A present the relative fluxes J_i of solute components S_1 and S_2. It is important to note that the ratios deviate from unity, being uniformly larger (at the co-solvent regime, $\Omega < 0$) or smaller (at the anti-solvent regime, $\Omega > 0$). Thus, neglecting the chemical interactions between diffusing components would result in over- or underestimation of the flux values. In the prescribed simulation conditions at $s_2 = s_1$, the corresponding fluxes become equal since all other model parameters (diffusion characteristics, molar masses, etc.) are assumed identical for both components. At smaller ratios s_2/s_1, the fluxes diverge, and in the limit of $s_2 \to 0$, the deviation from their corresponding "ideal" analogues increases up to 60%. The discrepancy level depends on the difference between $\overline{x}_i^*$ and $\overline{x}_i^0$, and $\overline{x}_i^* \approx \overline{x}_i^0$ only in a special case of $\Omega = 0$, when the fluxes become equal, $J_i \approx J_i^{sc}$.

The overall extraction rates, J_{12}, from an individual particle are depicted in Figure 6B. The flux J_{12} is of particular importance since it is the principal characteristic of the SFE process in the framework of the one-component solute approximation. The direct intercomparison of the one- and two-component models is not straightforward and relies on the choice of the apparent properties of the components. Nevertheless, one can compare the overall extraction rates predicted by the developed two-component model in its two limiting cases of the "ideal" (eqs 32−35) and "regular" (eqs 26−31) solutions. From Figure 6B, it becomes obvious that even chemical interactions between the three components in the solution can lead up to ∼30% changes in the overall flux. These variations depend on the s_2/s_1 ratio but become vanishingly small at $s_2 \ll s_1$. As demonstrated by Figure 6C, the flux of the solute component S_2 prevails over the fluxes of other components scaled by $\sim 1/s_i$.

4.3. Oil Precipitation in a Three-Component System. As a rule, it is assumed that the phase transition on the particle scale during SFE takes place only at the boundary between the SC and the transport zone. This assumption is reasonable for the one-component oil approximation. In the case of the two-component oil, the phase transition also continuously occurs within the subinterval $1 > z/as_1 > s_2/s_1$. This locally maintains the material equilibrium with respect to solute component S_2, $\mu_2(x_1, x_2) \equiv 0$, as discussed above and demonstrated in Figure 5A.

As predicted by the two-component oil model, the phase transitions can take place not only on the particle scale but also on the scale of the packed bed. The latter phenomenon is of particular importance and means that the "fluid" leaving the extractor may be a heterogeneous mixture.

The phase separation on the packed bed scale can occur in the "anti-solvent" regime at the two additional conditions. First, if, say, S_2 is the precipitating oil component, its concentration c_2 in the solvent has to increase at a higher rate than that of the concentration c_1, i.e., $dc_2/dt \gg dc_1/dt$, or, in other words, at $J_2 \gg J_1$ and $\mathcal{D}_{02} \gg \mathcal{D}_{01}$. From the other side, if $\Theta_1 = \Theta_2$, then this means that $s_2 \gg s_1$. As a result, at longer diffusion paths, the constraint $J_2 \gg J_1$ weakens, and the two fluxes become equal. Thus, as discussed below, the initial disbalance in the oil content, $\Theta_1 \neq \Theta_2$, is needed for the phase precipitation.

The second condition of the phase separation is related to the constraint on the lengths of the diffusion paths: $ds_2/dt < ds_1/dt$. In accordance with eq 31, this scenario is possible at $J_2/\Theta_2 < J_1/\Theta_1$ with $\Theta_2 > \Theta_1$. The detailed values of Θ_2 and Θ_1 are not discussed here. For instance, for further analysis illustrated by Figure 7, it is assumed that $\mathcal{D}_{02} = 4\mathcal{D}_{01}$ and $s_2/s_1 = 0.5$. The typical time scales of variations of concentrations c_i and transport zone lengths s_i have been deduced earlier in Section 3.6. In this case, a continuous disbalance in the components fluxes is maintained, with $J_2 \gg J_1$; the composition of the solvent phase $\{c_1; c_2\}$ follows the magenta curve and reaches the two-phase equilibrium in the packed bed (the triangular

https://doi.org/10.1021/acs.iecr.3c01488
Ind. Eng. Chem. Res. XXXX, XXX, XXX−XXX

marker in Figure 7) at $c_1 \ll c_2 \approx \overline{x}_1^* \approx \overline{x}_2^*$ rather than at $c_1 \approx c_2 \approx \overline{x}_1^* \approx \overline{x}_2^*$. The point $(\overline{x}_1^*; \overline{x}_2^*)$ is shown by the square marker in Figure 7A.

The solvent-phase composition $\{c_1(\tau); c_2(\tau)\}$ for the described scenario is shown in Figure 7A by the solid magenta curve, where time τ is a parameter along the curve. The curve starts at point (0;0), which is the initial (inlet) condition for the solvent-phase concentration at the pores of the packed bed. While the solvent travels through the porous medium along the packed bed, the concentration of the dissolved solute components increases. However, the diffusion rates of component S_2 are greater than those of S_1. A rapid initial increase of the solute component concentration c_2 is observed at a reasonably small concentration c_1. Furthermore, the magenta curve initially follows the x_2 coordinate axis.

Eventually the concentration trajectory in Figure 7A hits the blue curve, $c_1 = \overline{c}_1$, $c_2 = \overline{c}_2$, which shows the solvent-phase compositions in equilibrium with the oil phase composed of pure S_2. From this moment on, the constraint $\mu_2(\overline{c}_1, \overline{c}_2) \equiv 0$ is fulfilled in the pores of the packed bed, as well as inside the particles, $\mu_2(\overline{x}_1, \overline{x}_2) \equiv 0$. However, there is no material (diffusion) equilibrium with respect to the oil component S_1 yet, i.e., $\mu_1(\overline{c}_1, \overline{c}_2) < 0$, while $\mu_1 = 0$ at the SC surface $z = as_1$. The diffusion of pure oil component S_1 is still observed from the particles to the pores of the packed bed. The solvent-phase composition $(c_1; c_2)$ follows the blue curve and tends to the point $(\overline{x}_1^*; \overline{x}_2^*)$ shown by the green square in Figure 7A. It is a junction of the blue and the red curves, so $\mu_1(\overline{x}_1^*, \overline{x}_2^*) = 0$ and $\mu_2(\overline{x}_1^*, \overline{x}_2^*) = 0$ simultaneously.

To reach this equilibrium composition, the concentration of the dissolved oil molecules S_2 in the solvent phase must decrease following the blue curve. Moreover, the concentration c_1 increases accordingly due to the diffusion process. However, there is no diffusion of the oil component S_2, since its chemical potential is zero in the particles as well as in the packed bed. So, the only way for the component S_2 to decrease its concentration in the pores is to precipitate as an oil phase, and the multiphase heterogeneous mixture flows through the packed bed.

The corresponding time dependence of dissolved oil components concentrations c_1 and c_2 is shown by the solid curves in Figure 7B. The concentrations in the solvent phase are shown by the solid curves, while the dashed curves show the overall molar concentrations in the multiphase flowing fluid. At $\tau \approx 2.4$ (introduced in Section 3.6), the blue and the black solid curves split into a solid and a dashed part. Interestingly, in the simulated regime, the overall concentration $c_1 + c_2$ (shown by the black solid curve in Figure 7B) remains constant once the process reaches the two-phase equilibrium at $\tau \approx 2.4$. So, the amount of component S_1 that enters the packed bed pores is equal to the amount of component S_2 that precipitates from the solution.

Finally, the difference between the solid and dashed parts is the oil concentration that is precipitated as the oil phase. In this scenario, about 25% of the extracted oil component S_2 has precipitated.

5. CONCLUSIONS

Mathematical modeling of SFE processes based on the use of $scCO_2$ is very challenging. $scCO_2$ as a solvent is conventionally utilized for extracting the target components from natural products that are composed of many substances exhibiting different solubility. In this case, it is of primary importance to control the content of target compounds in the extract as well as the solvent consumption by properly chosen extraction conditions. However, in practice, the SFE procedure is often adjusted simply by experience rather than on the basis of valuable and reliable information delivered by mathematical models.[46] From this point of view, the new approach proposed and analyzed in this paper is aimed at developing sophisticated mathematical models of SFE which take into account the multicomponent nature of the extract and predict the evolution of the extract composition in the course of extraction. A particular case of two-component oil extraction is considered and extends the approaches of earlier publications to the regular solution approximation.

Previously developed models did not consider interaction between different species in the solution. It is shown that the particle-scale extraction rates crucially depend on the surrounding solution composition and thermodynamic properties of the oil and solute components that control the mass-transfer processes. It is demonstrated that in typical SFE conditions, the "regular solution" correction to the chemical potentials can lead to a 60% correction of the diffusion flux toward the particle surface. The correction to the overall flux J_{12} is not uniform with respect to the time-dependent model parameters, such as transport zone thicknesses s_1 and s_2. Thus, it is impossible to adjust the ideal and regular solution models by introducing apparent (effective) parameters.

As a rule of thumb, the effect of the regular solution correction, given by Ω, on the evolution of the solution concentrations c_1 and c_2 can be assessed through the difference of $\overline{x}_i^0$ and $\overline{x}_i^*$. The greater the difference, the more important the solute component interactions.

Unfortunately, the developed approach does not directly predict conditions of selective extraction of a particular component, alternately followed by extraction of the other component. Therefore, it is expected that the optimal and efficient way to selectively extract a particular oil component is to adjust pressure and temperature variations in the course of extraction to manipulate the solubilities $\overline{x}_i^0$ and $\overline{x}_i^*$.

AUTHOR INFORMATION

Corresponding Author

Artur A. Salamatin − *Institute of Mechanics and Engineering, FRC Kazan Scientific Center, Russian Academy of Sciences, Kazan 420111, Russia; Institute of Computational Mathematics and Information Technologies, Kazan Federal University, Kazan 420008, Russia;* orcid.org/0000-0002-1099-4016; Email: arthur.salamatin2@gmail.com, salamatin@imm.knc.ru; Fax: +7 (843) 236-52-89

Author

Alyona S. Khaliullina − *Institute of Fundamental Medicine and Biology, Kazan Federal University, Kazan 420008, Russia*

Complete contact information is available at: https://pubs.acs.org/10.1021/acs.iecr.3c01488

Notes

The authors declare no competing financial interest.

ACKNOWLEDGMENTS

This study was supported by the Russian Scientific Foundation through grant no. 22-71-00080. The numerical scheme implementation as a computer program was supported by

https://doi.org/10.1021/acs.iecr.3c01488
Ind. Eng. Chem. Res. XXXX, XXX, XXX−XXX

the Kazan Federal University Strategic Academic Leadership Program ("PRIORITY-2030").

NOMENCLATURE

a	half-thickness of the plane particle of the ground raw material
c	bulk solute concentration in the solvent phase around the particle
$Đ_{ij}$	Stefan−Maxwell (drag) diffusion coefficient between two species i and j
g	molar Gibbs energy that the oil molecule S_i gains upon transition from the oil phase (the reference state) to the solvent phase
G	Gibbs energy of a phase
j_i	scaled mass diffusion flux of species i
J_i	mass diffusion flux of species i
M	molar mass of an individual component
n	number of moles of molecules in the phase
N_j	molar flux of species j
R	universal gas constant
s	transport zone thickness normalized with respect to a
S_i	ith oil component
t	time
T	temperature
u	velocity of the diffusing species
x	molar concentration of the component in the phase
X_i	molar diffusion flux of species i relative to the molar average reference velocity u
Y	mass fraction of oil extracted from the packed bed to the time moment t
z	Cartesian coordinate introduced in every particle; z = 0 at the particle surface, and $z = a$ at the particle plane of symmetry
B	factor describing the drag between diffusing species
Γ	thermodynamic factor matrix
θ	mass density of oil component S_i dissolved in the solvent in the extraction conditions
Θ	initial content of pseudo-component S of extractable oil compounds per unit volume of the raw material
μ	chemical potential
τ	dimensionless time
Ω	S_1−S_2 binary interaction parameter within the solvent medium
Ω_i	solvent−S_i binary interaction parameter
BIC	broken-and-intact cell
OEC	overall extraction curve
MC-SC	multicomponent shrinking core (model)
SC	shrinking core
TAG	triacylglycerol

Subscripts

i	index of individual components
sc	characteristic scale of the process
t	total number of moles in the phase

Superscripts

(CO_2)	the quantity is related to the CO_2 solution phase
(oil)	the quantity is related to the oil phase
overbar	the quantity is related to the solution phase that is in equilibrium with the oil phase
*	three-phase equilibrium

REFERENCES

(1) Brunner, G.; Baumgartel, H.; Franck, E. U.; Grumbein, W. *Topics in Physical Chemistry - Gas Extraction*; Springer, 1994 , DOI: 10.1007/978-3-662-07380-3.

(2) Leung, D. Y. C.; Wu, X.; Leung, M. K. H. A Review on Biodiesel Production Using Catalyzed Transesterification. *Appl. Energy* **2010**, *87*, 1083−1095.

(3) Herrero, M.; Mendiola, J. A.; Cifuentes, A.; Ibáñez, E. Supercritical Fluid Extraction: Recent Advances and Applications. *J. Chromatogr. A* **2010**, *1217*, 2495−2511.

(4) Schütz, E. Supercritical Fluids and Applications − A Patent Review. *Chem. Eng. Technol.* **2007**, *30*, 685−688.

(5) Yin, J. Z.; Xu, Q. Q.; Wei, W.; Wang, A. Q. Experiments and Numerical Simulations of Supercritical Fluid Extraction for Hippophae Rhamnoides L Seed Oil Based on Artificial Neural Networks. *Ind. Eng. Chem. Res.* **2005**, *44*, 7420−7427.

(6) Salgin, U.; Korkmaz, H. A Green Separation Process for Recovery of Healthy Oil from Pumpkin Seed. *J. Supercrit. Fluids* **2011**, *58*, 239−248.

(7) Meyer, F.; Jaeger, P.; Eggers, R.; Stamenic, M.; Milovanovic, S.; Zizovic, I. Effect of CO2 Pre-Treatment on ScCO2 Extraction of Natural Material. *Chem. Eng. Process. Process Intensif.* **2012**, *56*, 37−45.

(8) Fiori, L. Supercritical Extraction of Sunflower Seed Oil: Experimental Data and Model Validation. *J. Supercrit. Fluids* **2009**, *50*, 218−224.

(9) Salgin, U.; Döker, O.; Çalimli, A. Extraction of Sunflower Oil with Supercritical CO2: Experiments and Modeling. *J. Supercrit. Fluids* **2006**, *38*, 326−331.

(10) Özkal, S. G.; Yener, M. E.; Bayındırlı, L. Mass Transfer Modeling of Apricot Kernel Oil Extraction with Supercritical Carbon Dioxide. *J. Supercrit. Fluids* **2005**, *35*, 119−127.

(11) Salamatin, A. A. Detection of Microscale Mass-Transport Regimes in Supercritical Fluid Extraction. *Chem. Eng. Technol.* **2017**, *40*, 829−837.

(12) Salamatin, A. A. Numerical Scheme for Non-Linear Model of Supercritical Fluid Extraction from Polydisperse Ground Plant Material: Single Transport System. In *IOP Conference Series: Materials Science and Engineering*; Institute of Physics Publishing, 2016; Vol. *158* , DOI: 10.1088/1757-899X/158/1/012081.

(13) del Valle, J. M. Extraction of Natural Compounds Using Supercritical CO2: Going from the Laboratory to the Industrial Application. *J. Supercrit. Fluids* **2015**, *96*, 180−199.

(14) Goto, M.; Roy, B. C.; Hirose, T. Shrinking-Core Leaching Model for Supercritical-Fluid Extraction. *J. Supercrit. Fluids* **1996**, *9*, 128−133.

(15) Bootello, M. A.; Garcés, R.; Martínez-Force, E.; Salas, J. J. Dry Fractionation and Crystallization Kinetics of High-Oleic High-Stearic Sunflower Oil. *JAOCS. J. Am. Oil Chem. Soc.* **2011**, *88*, 1511−1519.

(16) Sovová, H. Modeling of the Triacylglycerol Stereospecific Composition of Vegetable Oils: I. Comparison of Models for Triacylglycerol Assembly. *Eur. J. Lipid Sci. Technol.* **2022**, *124*, 2000392.

(17) Sovová, H.; Sajfrtová, M.; Stateva, R. P. A Novel Model for Multicomponent Supercritical Fluid Extraction and Its Application to Ruta Graveolens. *J. Supercrit. Fluids* **2017**, *120*, 102−112.

(18) Sovova, H.; Stateva, R. P. New Approach to Modeling Supercritical CO2 Extraction of Cuticular Waxes: Interplay between Solubility and Kinetics. *Ind. Eng. Chem. Res.* **2015**, *54*, 4861−4870.

(19) Goto, M.; Roy, B. C.; Kodama, A.; Hirose, T. Modeling Supercritical Fluid Extraction Process Involving Solute-Solid Interaction. *J. Chem. Eng. Jpn.* **1998**, *31*, 171−177.

(20) del Valle, J. M.; Urrego, F. A. Free Solute Content and Solute-Matrix Interactions Affect Apparent Solubility and Apparent Solute Content in Supercritical CO2 Extractions. A Hypothesis Paper. *J. Supercrit. Fluids* **2012**, *66*, 157−175.

(21) Prausnitz, J. M.; Lichtenthaler, R. N.; De Azevedo, E. G. *Molecular Thermodynamics of Fluid-Phase Equilibria*; Prentice Hall PTR, 1999.

https://doi.org/10.1021/acs.iecr.3c01488
Ind. Eng. Chem. Res. XXXX, XXX, XXX−XXX

(22) Durling, N. E.; Catchpole, O. J.; Grey, J. B.; Webby, R. F.; Mitchell, K. A.; Foo, L. Y.; Perry, N. B. Extraction of Phenolics and Essential Oil from Dried Sage (Salvia Officinalis) Using Ethanol−Water Mixtures. *Food Chem.* **2007**, *101*, 1417−1424.
(23) Egorov, A. G.; Salamatin, A. A. Bidisperse Shrinking Core Model for Supercritical Fluid Extraction. *Chem. Eng. Technol.* **2015**, *38*, 1203−1211.
(24) Salamatin, A. A. Supercritical Fluid Extraction of the Seed Fatty Oil: Sensitivity to the Solute Axial Dispersion. *Ind. Eng. Chem. Res.* **2020**, *59*, 18126−18138.
(25) Tezel, A.; Hortaçsu, A.; Hortaçsu, Ö. Multi-Component Models for Seed and Essential Oil Extractions. In *Journal of Supercritical Fluids*; Elsevier, 2000; Vol. *19*, pp. 3−17 , DOI: 10.1016/S0896-8446(00)00079-6.
(26) Teberikler, L.; Koseoglu, S. S.; Akgerman, A. Modeling of Selective Extraction of Phosphatidylcholine from a Complex Lecithin Mixture Using Supercritical CO2/Ethanol. *J. Food Lipids* **2003**, *10*, 203−218.
(27) Sundman, B.; Lu, X.-G.; Ohtani, H. The Implementation of an Algorithm to Calculate Thermodynamic Equilibria for Multi-Component Systems with Non-Ideal Phases in a Free Software. *Comput. Mater. Sci.* **2015**, *101*, 127−137.
(28) Gyarmati, I. *Non-Equilibrium Thermodynamics: Field Theory and Variational Principles*; Springer, 1970.
(29) Toor, H. L. Diffusion in Three-Component Gas Mixtures. *AIChE J.* **1957**, *3*, 198−207.
(30) Krishna, R.; Wesselingh, J. A. The Maxwell-Stefan Approach to Mass Tranfer. *Chem. Eng. Sci.* **1997**, *52*, 861−911.
(31) Taylor, R.; Krishna, R. *Multicomponent Mass Transfer*; John Wiley & Sons, Ltd, 1954.
(32) Calvignac, B.; Rodier, E.; Letourneau, J. J.; Dos Santos, P. M. A.; Fages, J. Cocoa Butter Saturated with Supercritical Carbon Dioxide: Measurements and Modelling of Solubility, Volumetric Expansion, Density and Viscosity. *Int. J. Chem. React. Eng.* **2010**, *8* (), DOI: 10.2202/1542-6580.2191.
(33) Privat, R.; Jaubert, J.-N.; Berger, E.; Coniglio, L.; Lemaitre, C.; Meimaroglou, D.; Warth, V. Teaching the Concept of Gibbs Energy Minimization through Its Application to Phase-Equilibrium Calculation. *J. Chem. Educ.* **2016**, *93*, 1569−1577.
(34) Alvarez-Montaño, V. E.; Farías, M. H.; Brown, F.; Muñoz-Palma, I. C.; Cubillas, F.; Castillón-Barraza, F. F. Phase Relations in Ternary Systems in the Subsolidus Region: Methods To Formulate Solid Solution Equations and To Find Particular Compositions. *J. Chem. Educ.* **2017**, *94*, 1247−1254.
(35) Furse, S.; Liddell, S.; Ortori, C. A.; Williams, H.; Neylon, D. C.; Scott, D. J.; Barrett, D. A.; Gray, D. A. The Lipidome and Proteome of Oil Bodies from Helianthus Annuus (Common Sunflower). *J. Chem. Biol.* **2013**, *6*, 63.
(36) Egorov, A. G.; Mazo, A. B.; Maksudov, R. N. Extraction from a Polydisperse Granular Layer of Milled Oilseeds with Supercritical Carbon Dioxide. *Theor. Found. Chem. Eng.* **2010**, *44*, 642−650.
(37) Döker, O.; Salgin, U.; Yildiz, N.; Aydoğmuş, M.; Çalimli, A. Extraction of Sesame Seed Oil Using Supercritical CO2 and Mathematical Modeling. *J. Food Eng.* **2010**, *97*, 360−366.
(38) Leonardi, E.; Angeli, C. On the Maxwell - Stefan Approach to Diffusion: A General Resolution in the Transient Regime for One-Dimensional Systems. *J. Phys. Chem. B* **2010**, *114*, 151−164.
(39) Ma, Y.; Zhang, F.; Deckman, H. W.; Koros, W. J.; Lively, R. P. Flux Equations for Osmotically Moderated Sorption-Diffusion Transport in Rigid Microporous Membranes. *Ind. Eng. Chem. Res.* **2020**, *59*, 5412−5423.
(40) Salamatin, A. A. Estimation of the Axial Dispersion Effect on Supercritical Fluid Extraction from Bidisperse Packed Beds. *Russ. J. Phys. Chem. B* **2017**, *11*, 1180−1187.
(41) Janzen, T.; Vrabec, J. Diffusion Coefficients of a Highly Nonideal Ternary Liquid Mixture: Cyclohexane-Toluene-Methanol. *Ind. Eng. Chem. Res.* **2018**, *57*, 16508−16517.
(42) Ren, W.; Li, G.; Tian, S.; Sheng, M.; Geng, L. Adsorption and Surface Diffusion of Supercritical Methane in Shale. *Ind. Eng. Chem. Res.* **2017**, *56*, 3446−3455.
(43) Salamatin, A. A.; Haliullina, A. S. Characteristic Scales of the Supercritical-Fluid Extraction Process. *Theor. Found. Chem. Eng.* **2022**, *56*, 742−753.
(44) Promraksa, A.; Siripatana, C.; Rakmak, N.; Chusri, N. Modeling of Supercritical CO2 Extraction of Palm Oil and Tocopherols Based on Volumetric Axial Dispersion. *J. Supercrit. Fluids* **2020**, *166*, No. 105021.
(45) Sovová, H. Broken-and-Intact Cell Model for Supercritical Fluid Extraction: Its Origin and Limits. *J. Supercrit. Fluids* **2017**, *129*, 3−8.
(46) Salamatin, A. A.; Haliullina, A. S. Evaluation of Supercritical Fluid Extraction Model Parameters by Monte-Carlo Methods. *Theor. Found. Chem. Eng.* **2022**, *56*, 69−83.

https://doi.org/10.1021/acs.iecr.3c01488
Ind. Eng. Chem. Res. XXXX, XXX, XXX−XXX